Available online at www.sciencedirect.com

ScienceDirect

MATTER AND RADIATION AT EXTREMES

Matter and Radiation at Extremes 2 (2017) 28–36

www.journals.elsevier.com/matter-and-radiation-at-extremes

Research Article

On intense proton beam generation and transport in hollow cones

J.J. Honrubia [a,*], A. Morace [b], M. Murakami [b]

[a] *ETSI Aeronáutica y del Espacio, Universidad Politécnica de Madrid, Madrid, Spain*
[b] *Institute of Laser Engineering, Osaka University, Osaka, Japan*

Received 14 October 2016; revised 3 November 2016; accepted 8 November 2016
Available online 8 December 2016

Abstract

Proton generation, transport and interaction with hollow cone targets are investigated by means of two-dimensional PIC simulations. A scaled-down hollow cone with gold walls, a carbon tip and a curved hydrogen foil inside the cone has been considered. Proton acceleration is driven by a 10^{20} W·cm^{-2} and 1 ps laser pulse focused on the hydrogen foil. Simulations show an important surface current at the cone walls which generates a magnetic field. This magnetic field is dragged by the quasi-neutral plasma formed by fast protons and co-moving electrons when they propagate towards the cone tip. As a result, a tens of kT B_z field is set up at the cone tip, which is strong enough to deflect the protons and increase the beam divergence substantially. We propose using heavy materials at the cone tip and increasing the laser intensity in order to mitigate magnetic field generation and proton beam divergence.

PACS Codes: 52.38.Kd; 52.65.Ww; 52.57.Kk

Keywords: Inertial fusion energy; Ion fast ignition; Laser driven ion acceleration

1. Introduction

Proton acceleration by laser beams is a subject of interest for many potential applications which cover a wide range, from cancer therapy [1] to high energy density matter studies [2], including fast ignition of inertial fusion capsules [3,4]. The target normal sheath acceleration (TNSA) scheme [5] has been widely studied by several authors over the last 15 years. Just after the first experimental evidence of proton acceleration by the TNSA scheme, fast ignition (FI) of inertial fusion capsules by laser-driven protons was proposed [6]. This was followed by theoretical studies on the TNSA scheme [7,8], target studies [9–11], new irradiation schemes [12–14] and the use of ions heavier than protons [15,16]. One of the main advantages of proton FI is its high laser-to-proton conversion efficiency which can be as high as 15% as it has been demonstrated in recent experiments [17].

The standard proton fast ignition scheme assumes that the proton beam is generated inside a hollow cone attached to an inertial fusion capsule by means of the TNSA scheme [18]. Most of the proton FI calculations carried out so far are based on the strong assumptions of ideal perfectly collimated beams and optimal target configurations, which clearly under-estimate the laser energy requirements for ignition. Other studies [19] assumed that proton acceleration and transport within the cone takes place in an ideal manner, i.e. protons are focused on the cone tip and emerge with a given divergence angle. In addition, it is widely assumed that there are not any relevant interactions between the proton beam and the cone tip. Only recently, collective stopping of ion beams in solid matter has been reported [20].

Beam focusing is one of the key issues of proton FI. Some focusing techniques have been developed for laser-driven protons such as ballistic transport [21,22], magnetic lenses [23–25], self-generated fields in hollow microcylinders illuminated by intense sub-picosecond laser pulses [26] and

* Corresponding author.
E-mail address: javier.honrubia@upm.es (J.J. Honrubia).
Peer review under responsibility of Science and Technology Information Center, China Academy of Engineering Physics.

http://dx.doi.org/10.1016/j.mre.2016.11.001

achromatic electrostatic lenses [27]. Offermann et al. [28] found theoretically and experimentally that ion divergence depends on the thermal expansion of the co-moving hot electrons, resulting in a hyperbolic ion beam envelope. Using these results, Bartal et al. demonstrated experimentally an enhanced focusing of TNSA protons in cone targets, predicting spot diameters about 20 μm for proton FI conditions [29], well under the 40 μm spots required [14,19]. The focusing mechanism reported by Bartal et al. is based on the onset of an electron sheath near the cone walls, which generates the electrostatic fields to focus the proton beam on the cone tip.

In this paper, proton generation, transport and interaction with the cone tip are studied by means of two-dimensional (2D) PIC simulations. A scaled-down hollow cone with gold walls, a carbon tip and a curved hydrogen foil inside the cone has been considered. Proton acceleration is driven by a 10^{20} $W\cdot cm^{-2}$ and 1 ps laser pulse focused on the converter foil. The cone is surrounded by a deuterium-tritium (DT) low density plasma mimicking the imploded shell of the standard cone-targets used in fast ignition. It is worth pointing out that the cone tip and the surrounding DT plasma have not been considered so far in studies of proton acceleration in hollow cones despite they play an important role in the beam neutralization and divergence.

This article is organised as follows. In Section 2, the data used in PIC simulations are described. Section 3 summarises the results obtained for the proton beam generation and transport within a standard cone design. Next, in Section 4, it is proposed using heavy elements in the cone tip and higher intensity laser pulses in order to mitigate the magnetic field growth and the subsequent beam deflection at the cone tip. Finally, conclusions and future work are summarized in Section 5.

2. Simulation model

Proton beam generation and transport simulations have been performed by means of the 2D PIC code EPOCH [30]. We assume that a highly uniform laser beam impinges on a curved hydrogen foil (the converter) placed inside a hollow cone. Following the standard proton fast ignition scheme [31], the cone is formed by gold walls and a carbon tip in order to mitigate the proton beam scattering and energy losses found for high-Z materials [19]. The cone is cold initially. However, a mean charge state of +18 has been assumed for the gold walls and full ionization for the carbon tip, which are kept constant during the whole simulation. The electron density of the cone tip and walls is set to $100n_c$, where $n_c = 1.1 \times 10^{21}$ cm^{-3} is the critical density for a laser beam with a wavelength $\lambda = 1$ μm. The masses of the Au^{18+} and C^{6+} ions are set to $197m_p$ and $12m_p$, respectively, where m_p is the proton rest mass. The cone opening half-angle is 20° and it is surrounded by a fully ionized deuterium-tritium plasma with an electron density of $10n_c$ and an ion mass of $2.5m_p$. The cone walls and the tip thicknesses are 5 μm and 8 μm, respectively. The simulation box used is shown in Fig. 1. The converter is a 3.5-μm-thick hydrogen foil with an electron density of $100n_c$ and a pre-plasma sited at the laser side with an exponential profile, $\exp(-r/l)$, where r is the radius and $l = 2$ μm the scale-length. The curvature radius of the converter is 65 μm and it is centered at $x = 85$ μm, the middle of the cone tip. We assume that initially the converter foil and the surrounding DT are fully ionized and cold.

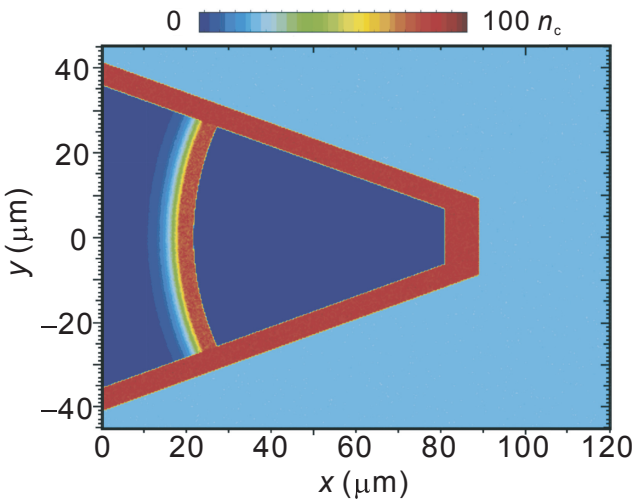

Fig. 1. Initial electron density distribution for PIC simulations. The laser pulse comes from the left.

The size of the simulation box is 120 μm × 90 μm in the x and y directions, respectively. The cell width is 0.0286 μm in each direction, which corresponds to 35 cells per laser wavelength. The total number of particles in the simulation box is 7.5×10^8.

A p-polarized laser pulse impinges on the left side of the simulation box. The laser wavelength is $\lambda = 1$ μm and the peak intensity $I_{max} = 10^{20}$ $W\cdot cm^{-2}$ (normalized vector potential $a_0 = 7.25$). The laser intensity is given by $I = I_{max}\exp[-(y/\sigma)^4]\exp\{-[(t-t_0)/\tau]^2\}$, where $\sigma = 30$ μm, $\tau = 0.6$ ps and $t_0 = 0.6$ ps. A highly uniform laser beam with a super-Gaussian radial distribution has been selected to improve the ion beam focusing [32].

Periodic boundary conditions have been chosen for particles and fields in the y direction, while laser (fields outflow, laser inflow) and thermal conditions are used at the left and right boundaries, respectively. Coulomb collisions have not been taken into account in the simulations shown in the next Sections.

3. Proton acceleration and transport in standard hollow cones

Fast electrons are generated in the pre-plasma region next to the converter foil and propagate almost at the speed of light towards the cone walls and the surrounding DT plasma. The fast electron temperature at the time of the peak laser intensity (0.6 ps, 10^{20} $W\cdot cm^{-2}$) is 4.5 MeV, which is higher but close to the ponderomotive scaling (3.9 MeV). As expected for the thick foil used in our simulations (3.5 μm), protons are accelerated at the foil rear surface by the TNSA mechanism

with the difference that, actually, the quasi-neutrality of the converter foil is maintained not only by the refluxing fast electrons from the rear foil surface, but also by the electrons moving from the cone walls and the surrounding DT to the foil, as shown in Fig. 2. As a result, a surface current in the cone walls directed towards the tip is set up generating a B_z magnetic field, whose consequences will be analyzed in the next sections. The laser-to-proton conversion efficiency found in this case is about 7% and the proton mean energy in a plane sited at $x = 91$ μm, just after the cone tip, is 3.3 MeV.

The longitudinal electric field E_x and the transverse electric field E_y averaged over a laser period at 0.5 ps are shown in Fig. 3. The E_x field is generated by the charge separation induced by fast electrons trying to escape through the foil rear surface. The accelerated protons are neutralized in charge and current by the co-moving fast electrons, creating a quasi-neutral plasma which propagates towards the cone tip. The B_z field generated initially near the converter rear surface is dragged by this quasi-neutral plasma, as will be discussed in the next paragraphs. This B_z field together with the E_x field cause that most of the fast electrons reflux across the converter while a smaller fraction flows along the converter rear surface. This surface current propagates and continues flowing along the cone inner surface towards the tip [33].

The transverse electric field E_y averaged over a laser period at 0.5 ps is plotted in Fig. 3(b). Similarly to the development of the E_x field at the converter rear surface, the E_y field is generated by the fast electrons trying to pass through the cone wall vacuum interface. Nevertheless, as gold ions are much heavier than protons, their acceleration towards the axis is not as important. As a result, fast electrons are trapped in the wall due to the E_y and B_z fields setting up a surface current directed towards the cone tip. On the contrary, the E_y field pushes the accelerated protons towards the cone axis, focusing them in a diameter smaller than the tip. Later on, when the laser is off and the E_y field is lower, the focusing diameter increases up to almost the tip diameter. Hence, the beam focusing is a dynamic process changing the beam diameter from a few microns at the beginning of the proton pulse to the inner radius of the cone tip after the end of the pulse.

The relatively low laser-to-proton conversion efficiency (≈7%) found in our collisionless PIC simulation can be explained by the free flow of fast electrons and wall currents in our simulation, which reduces the sheath electron density at the converter rear surface and, thus, the accelerating electric field E_x, as it was reported by Qiao et al. [33]. A remedy for this is to add an insulator material between the converter foil and the cone walls in order to reduce the electron flow coming from the cone and even from the surrounding DT. However, as the increase of conversion efficiency takes place at the expense of beam focusing, a balance between both trends should be found for ignition-scale cone-target designs.

The evolution of the B_z field is plotted in Fig. 4, where the generation of magnetic field at the cone walls by the surface currents is shown, as it was anticipated by Zou et al. [34]. It is interesting to note how the B_z field generated near the walls and near the converter rear surface is dragged by the quasi-neutral plasma formed by the accelerated protons and co-moving electrons when travelling towards the cone tip. The amplification of the B_z field when frozen in a moving plasma is given by the induction equation, which for a collisionless plasma reads:

$$\frac{\partial \boldsymbol{B}}{\partial t} = \nabla \times (\boldsymbol{v} \times \boldsymbol{B}). \tag{1}$$

According to this equation, when the quasi-neutral plasma reaches the cone tip, the plasma velocity $\boldsymbol{v}$ drops to almost zero and the B_z field does not propagate further. In addition, the B_z amplification is a consequence of the magnetic flux conservation derived from Eq. (1). It is important to point out that the polarity and strength of the B_z field near the cone tip is such that it bends the trajectory of the protons, de-collimating the beam and raising its divergence. It is even possible that the B_z field hollows the proton beam, generating a ring shaped beam. This effect has been corroborated in experiments carried out at the Institute of Laser Engineering (ILE), Osaka University, Japan, where beam hollowing was measured in standing alone gold cones illuminated by 1.5 ps laser pulses with an intensity of 10^{19} W·cm^{-2} [35].

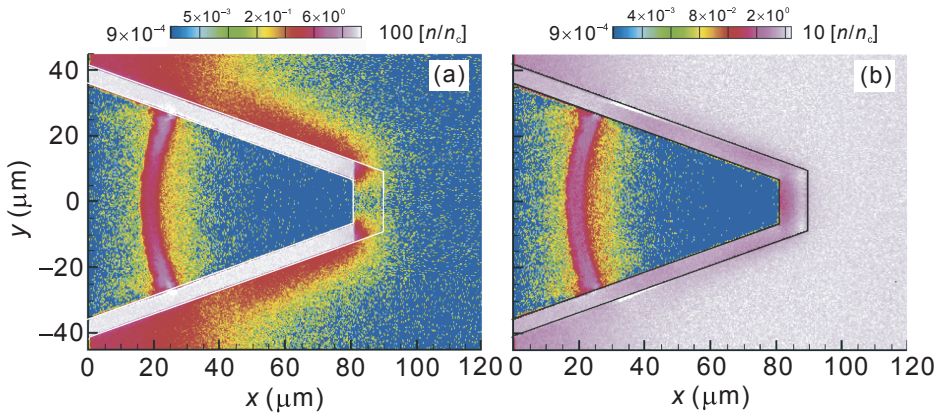

Fig. 2. (a) Density distribution of electrons from the cone walls and (b) surrounding DT plasma at 0.8 ps. The initial position of the cone edges is also depicted.

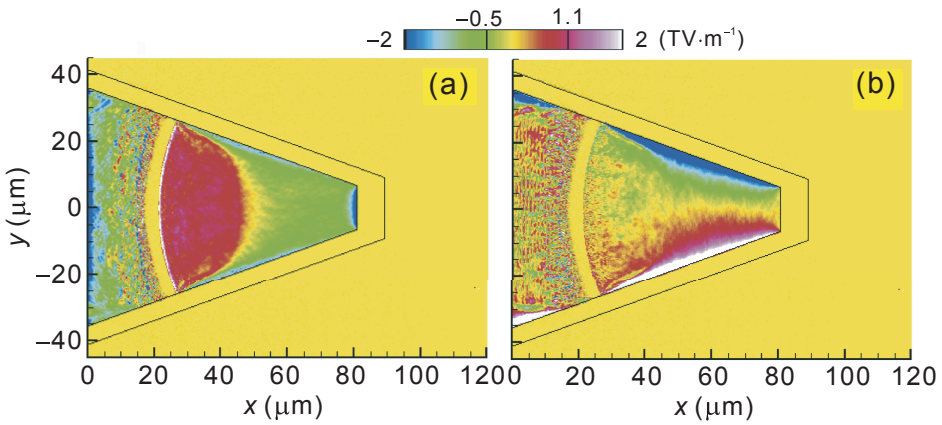

Fig. 3. Distributions of the electric field averaged over a laser period at 0.5 ps. (a) Longitudinal electron field E_x and (b) transverse electric field E_y.

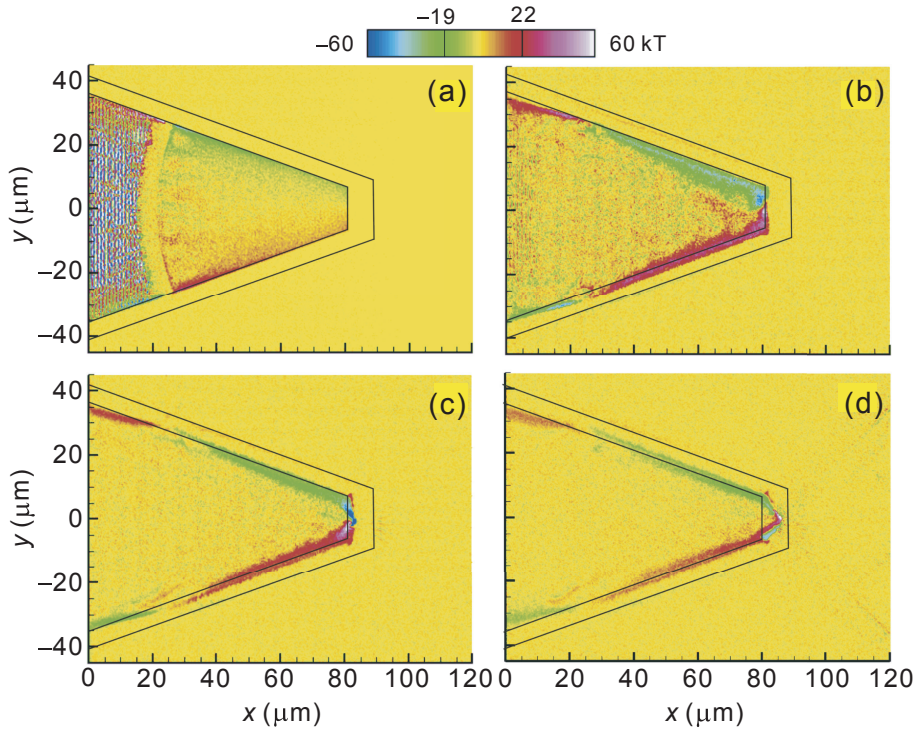

Fig. 4. B_z field distributions at (a) 0.5 ps, (b) 1.5 ps, (c) 2.5 ps and (d) 3.5 ps.

In addition to the increase of the beam divergence, the B_z field at the cone tip affects also the proton beam neutralisation. As a fraction of the co-moving electrons are trapped at the cone tip by the B_z field, the beam neutralizaton depends on the electrons provided by the tip and mainly by the surrounding DT to make possible the proton beam propagation.

The proton beam energy density obtained in our simulations is shown in Fig. 5, where an increase of the beam divergence and beam hollowing can be observed. It is worth noting that despite the proton beam is focused by the cone into a diameter similar to the cone tip or lower, the strong erosion of the carbon cone tip thickness compresses the B_z field, even more (see Fig. 4(d)), increasing its strength and resulting in the abovementioned beam hollowing and a substantial raise of its divergence.

The radial and angular distributions of protons just before and after the cone tip are shown in Fig. 6. The selected time of 2.0 ps and 3.5 ps corresponds to a beam power of 85% and 40% of its peak value (attained at 1.6 ps), a beam energy of 33% and 70% of the total beam energy, and a proton mean kinetic energy of 10.3 MeV and 2.7 MeV, respectively. It is interesting to note the evolution of the beam radial profiles from Gaussian to hollow when passing through the tip due to the B_z field. In both cases, the beam diameter is similar or smaller than the tip diameter ($\approx$14 μm), so that the cone fulfills perfectly its role of focusing the proton beam. We can also observe in Fig. 6(b) how the angular distribution is Gaussian before the tip with an increasing divergence with time. Just after the tip, the proton angular distribution is still Gaussian at 2 ps, while is strongly distorted at 3.5 ps by the B_z field at the

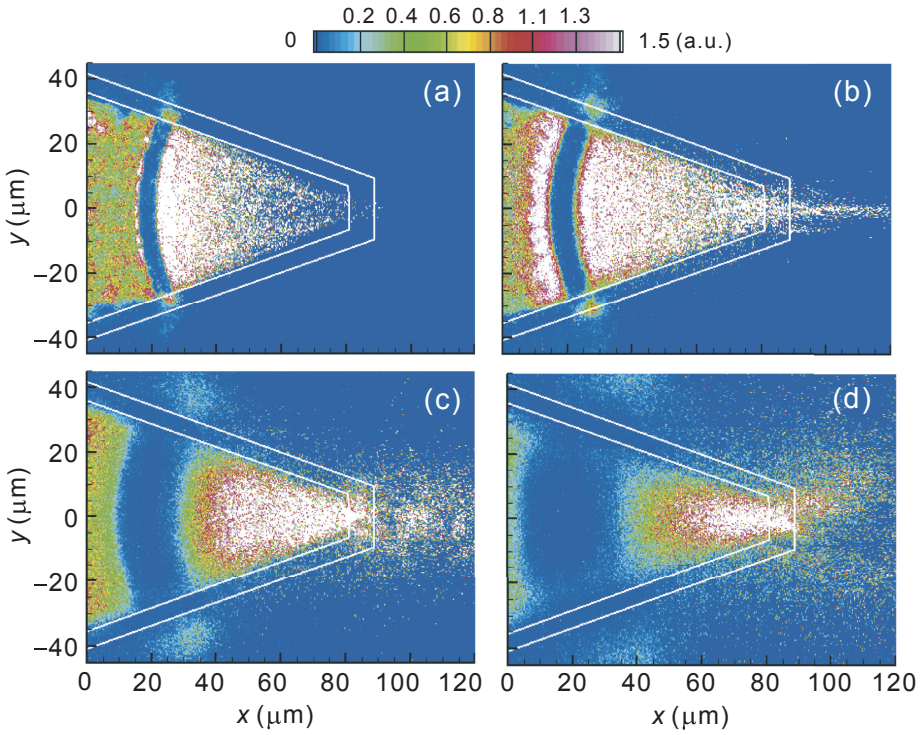

Fig. 5. Energy density of the proton beam at (a) 1.0 ps, (b) 1.5 ps, (c) 2.5 ps and (d) 3.5 ps.

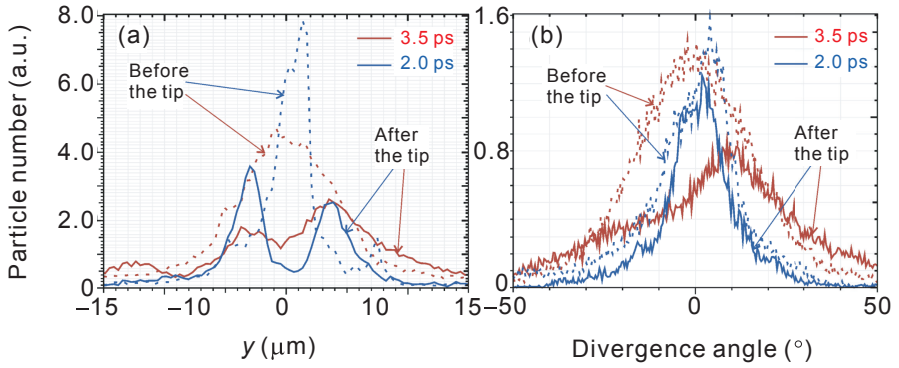

Fig. 6. (a) Radial and (b) angular distributions of the proton beam just before ($x = 79$ μm) and after ($x = 91$ μm) the cone tip at selected times. The distributions before and after the cone tip are plotted by dashed and solid lines, respectively.

tip (see Fig. 4(d)), as shown in Fig. 6(b). At this time, the beam divergence is quite high, with a full width at half maximum (FWHM) of about 55°.

4. Reduction of the beam divergence

As the B_z field is generated by the surface currents along the cone walls, the control of these currents can be effective for reducing the beam divergence. This could be done by isolating partially the converter foil from the cone walls by using high resistivity materials. In addition, this procedure has the advantage of improving the laser-to-proton conversion efficiency, as mentioned in Section 3. However, due to the extensive computational resources requested for doing multi-ps PIC simulations including collisions, we study here the dependence of the beam focusing on basic parameters of the cone target and the laser pulse, such as the cone tip material and the laser intensity. Advanced cone designs including collisional PIC simulations will be a subject of future studies.

4.1. Reduction of the beam divergence by using heavy materials at the cone tip

As shown in Section 3, the strong erosion of the carbon cone tip at the end of the proton pulse increases the beam divergence substantially. Thus, we have explored the possibility of reducing the tip erosion by using a heavier material at the cone tip. We have conducted PIC simulations of the same hollow cone depicted in Fig. 1 but with a gold tip. The electron densities near the carbon and gold cone tips are

plotted in Fig. 7, where it is shown how the strong erosion of the carbon tip (see Fig. 7(a)), is substantially reduced by using a gold tip (see Fig. 7(b)), and even more by using a gold cone tip and higher laser intensities (see Fig. 7(c)). The evolution of the proton beam energy density in the case of Fig. 7(b), with a gold cone tip and an energy of 10^{20} $W\cdot cm^{-2}$, can be seen in Fig. 8, where the reduction of the beam divergence is evidenced. Again, the beam is well collimated and focused for the highest energy protons (23 MeV at 1.5 ps) while it is deflected by the B_z field presented at the cone tip for lower energy protons (2.7 MeV at 3.5 ps).

Despite that the use of heavy materials at the cone tip improves the beam focusing, it has the drawback that Coulomb collisions between the beam protons and the tip, not taken into account in the PIC simulations shown here, will result in proton scattering and energy loss. The consequences of using high-Z elements at the cone tip in the proton fast ignition scenario have been quantified recently in Ref. [19], where it is shown that replacing a 25 μm carbon tip by a gold tip of the same thickness increases by 30% of the minimum ignition energy of a proton beam with a temperature of 7 MeV. Therefore, to improve the proton beam focusing by using heavy elements has a non-negligible cost in the laser beam requirements. Of course, the two opposite trends of beam focusing and ignition threshold should be balanced to minimize the laser beam energy requirements in a proton fast ignition point design.

4.2. Reduction of the beam divergence by increasing the laser intensity

In order to reduce the proton beam divergence further, we have explored the possibility to raise the laser intensity while keeping the pulse energy constant. Higher laser intensities will lead to higher proton temperatures and shorter interaction times, which in turn will give rise to lower deflection of protons and a lower generation of B_z field at the rear surface of the converter foil. Hence, both effects will contribute positively to proton beam focusing.

The effect of laser intensities higher than 10^{20} $W\cdot cm^{-2}$ has been analyzed by conducting a set of simulations of the cone shown in Fig. 1, with a gold tip driven by Gaussian laser pulses with peak intensities from 10^{20} $W\cdot cm^{-2}$ to 3×10^{20} $W\cdot cm^{-2}$ and pulse durations from 1 ps to 0.33 ps, respectively. In these cases, the laser absorption fraction increases from 0.67 to 0.73, the laser-to-proton conversion efficiency from 7% to 12%, and the proton mean kinetic energy from 3.3 MeV to 5.8 MeV when the peak laser intensity increases from 10^{20} $W\cdot cm^{-2}$ to 3×10^{20} $W\cdot cm^{-2}$, respectively. Our simulation results are plotted in Fig. 9, where a stable beam propagation is shown. Note that the divergence angle in Fig. 9 is lower than those in Figs. 5 and 8. Even low energy protons (2.7 MeV at 3.5 ps) form an almost uniform beam with a divergence half-angle around 15° (half width at half maximum).

The dependence of the beam divergence on the laser intensity is analyzed in Fig. 10. It is interesting to note that the proton angular distribution just before the cone tip is similar for the three laser intensities analysed. They have a Gaussian shape with a FWHM around 30°. However, just after the cone tip, there is a substantial difference between the divergences obtained for different laser intensities, which can be explained by the magnetic fields at the cone tip. For peak laser intensities of 2 $W\cdot cm^{-2}$ and 3×10^{20} $W\cdot cm^{-2}$, the angular distribution just after the cone tip has a Gaussian profile with the FWHM around 30°, while for 10^{20} $W\cdot cm^{-2}$ it raises up to 40° (FWHM), lower than the 55° (FWHM) found for a carbon cone tip with the same thickness and laser intensity. The role played by the cone tip in the deflection of the proton beam is evidenced by comparing Fig. 10(a) and (b). It is worthwhile pointing out that protons inside the cone have a Gaussian distribution with a spread depending, in principle, on the cone opening angle. This distribution is distorted by the B_z field cumulated at the tip, specially for the case of 10^{20} $W\cdot cm^{-2}$. Our results show that this distortion can be mitigated by using

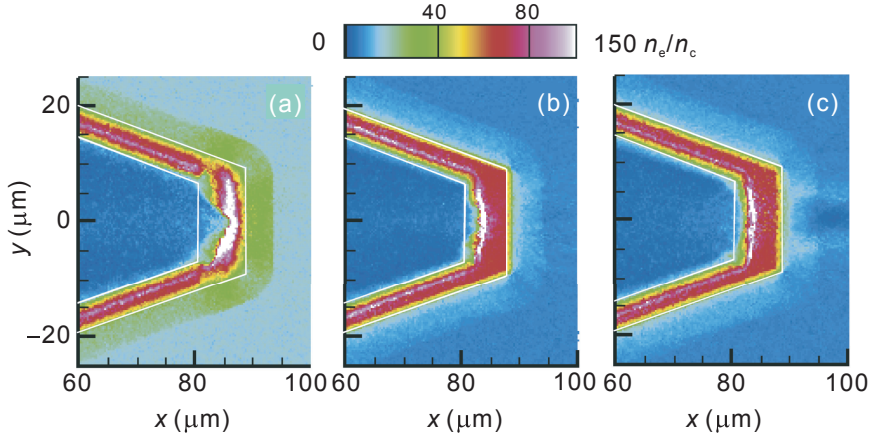

Fig. 7. Electron density distribution near the cone tip at 3.5 ps for the targets with (a) carbon cone tip and peak laser intensity of 10^{20} $W\cdot cm^{-2}$, (b) gold cone tip and peak laser intensity of 10^{20} $W\cdot cm^{-2}$, and (c) gold cone tip and peak laser intensity of 3×10^{20} $W\cdot cm^{-2}$.

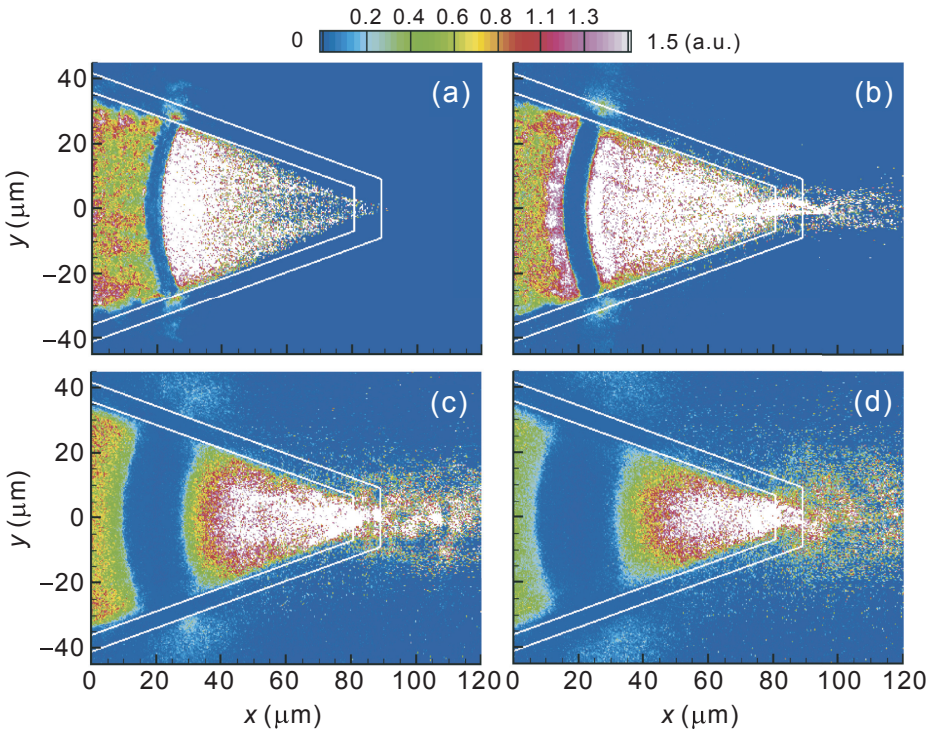

Fig. 8. Energy density of the proton beam at (a) 1.0 ps, (b) 1.5 ps, (c) 2.5 ps and (d) 3.5 ps for the target of Fig. 1, but with a cone tip of solid gold. The peak laser intensity is 10^{20} W·cm^{-2}.

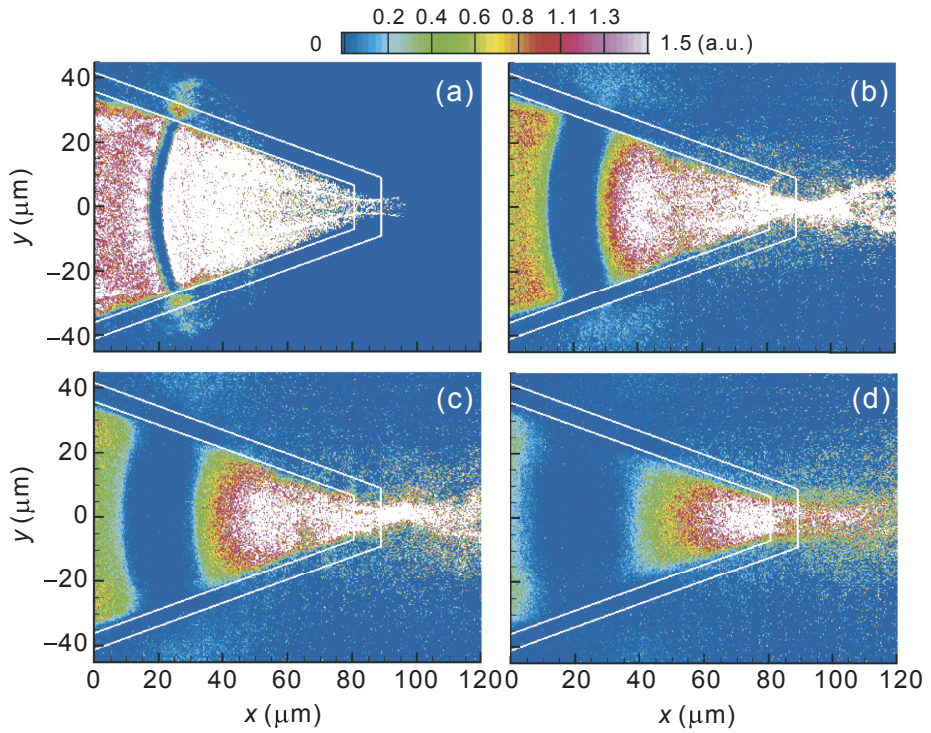

Fig. 9. Energy density of the proton beam at (a) 1.0 ps, (b) 1.5 ps, (c) 2.5 ps and (d) 3.5 ps for the target depicted in Fig. 1, but with a gold cone tip and illuminated by a laser pulse with a peak intensity of 3×10^{20} W·cm^{-2}.

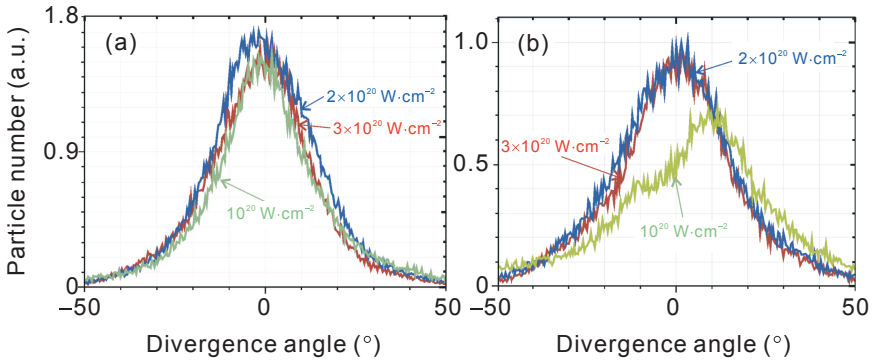

Fig. 10. Angular distribution of the proton beam at 3.5 ps just (a) before ($x = 79$ μm) and (b) after ($x = 91$ μm) the gold cone tip as a function of the peak laser intensity.

laser pulses with intensities higher than the standard 10^{20} $W \cdot cm^{-2}$ and high-Z materials at the cone tip.

5. Conclusions

Previous analyses have evidenced that the proton fast ignition calculations carried out so far have been optimistic regarding the distribution function of protons assumed and, in particular, its angular divergence [19]. Most of the analyses are based on perfectly collimated proton beams depositing their energy in a high density, isochoric DT core without surrounding plasmas [13]. Those analyses have motivated the study presented here, which is a characterisation of the proton source in the FI scenario by means of 2D PIC simulations. Our study is still preliminary because we are still far from a full characterization of the proton source for FI. Nevertheless, we have obtained relevant conclusions. The most important one to point out is that the surface currents at the cone walls generate a strong B_z field, which is dragged towards the cone tip and is amplified to high enough values of several tens of kT, to increase the proton beam divergence and, hence, the laser pulse energy requirements. Thus, controlling this source of proton divergence is of primary interest for fast ignition.

In this paper, we have proposed two actions for reducing the beam divergence: (1) using high-Z elements at the cone tip in order to avoid important tip erosion by making it more rigid and (2) using laser intensities higher than the standard 10^{20} $W \cdot cm^{-2}$ proposed for proton FI. Using heavy elements at the tip should be accompanied by the selection of the optimal material to fulfill the contradictory requirements of low beam divergence by using high-Z cone tips and minimum proton scattering due to Coulomb collisions by using low-Z elements. Increasing the laser intensity seems to be appropriate for reducing the proton beam divergence. However, it has to be demonstrated for the ~10 ps pulses required for proton FI. In general, the extension of our results to energies of tens of kJ and pulse durations of a few tens of picoseconds is still a task not affordable today by PIC simulations with present computer resources. Anyway, PIC simulations of ion acceleration and transport in cones are crucial to assess the feasibility of proton FI.

Our future work will be to perform integrated simulations of fast ignition with a more realistic proton source obtained from PIC simulations in order to have better estimations of the laser pulse required for the standard proton FI scheme based on TNSA. More advanced schemes such as the breakout-afterburner (BOA) [36] or the radiation pressure acceleration (RPA) [37] schemes should be investigated for the fast ignition scenario in order to minimize the laser beam requirements.

Acknowledgments

This work has been partially supported by the grant number ENE2014-54960-R of the Spanish Ministry of Economy and Competitiveness, the COST Action MP1208 and the Co-ordinated Research Project of IAEA F13016. We acknowledge the resources and technical assistance provided by the CeSViMa of the Polytechnic University of Madrid and the Barcelona Supercomputing Centre, both of the Spanish Supercomputing Network.

References

[1] U. Linz, J. Alonso, What will it take for laser driven proton accelerators to be applied to tumor therapy? Phys. Rev. STAB 10 (2007) 094801 http://dx.doi.org/10.1103/PhysRevSTAB.10.094801.
[2] S. Palaniyappan, C. Huang, D.C. Gautier, C.E. Hamilton, M.A. Santiago, et al., Efficient quasi-monoenergetic ion beams from laser-driven relativistic plasmas, Nat. Commun. 6 (2015) 10170, http://dx.doi.org/10.1038/ncomms10170.
[3] M. Tabak, J. Hammer, M.E. Glinsky, W.L. Kruer, S.C. Wilks, et al., Ignition and high gain with ultrapowerful lasers, Phys. Plasmas 1 (1994) 1626, http://dx.doi.org/10.1063/1.870664.
[4] M. Tabak, D. Callahan-Miller, Design of a distributed radiator target for inertial fusion driven from two sides with heavy ion beams, Nucl. Instr. Meth. 415 (1998) 75, http://dx.doi.org/10.1016/S0168-9002(98)00371-4.
[5] R.A. Snavely, M.H. Key, S.P. Hatchett, T.E. Cowan, M. Roth, et al., Intense high-energy proton beams from petawatt-laser irradiation of solids, Phys. Rev. Lett. 85 (2000) 2495, http://dx.doi.org/10.1103/PhysRevLett.85.2945.
[6] M. Roth, T.E. Cowan, M.H. Key, S.P. Hatchett, C. Brown, et al., Fast ignition by intense laser-accelerated proton beams, Phys. Rev. Lett. 86 (2001) 436, http://dx.doi.org/10.1103/PhysRevLett.86.436.
[7] P. Mora, Plasma expansion into a vacuum, Phys. Rev. Lett. 90 (2003) 185002, http://dx.doi.org/10.1103/PhysRevLett.90.185002.
[8] M. Murakami, M.M. Basko, Self-similar expansion of finite-size non-quasi-neutral plasmas into vacuum: Relation to the problem of ion

acceleration, Phys. Plasmas 13 (2006) 012105, http://dx.doi.org/10.1063/1.2162527.

[9] S. Hatchett, O.S. Jones, M. Tabak, R.E. Turner, R.B. Stephens, Cone-focused fast ignition: Sub-ignition proof-of-principle experiments, in: M. Key (Ed.), Contribution to the 6th Workshop on Fast Ignition of Fusion Targets, 16−19 November 2002, St. Petes Beach, Florida, USA, 2002.

[10] S. Atzeni, M. Temporal, J.J. Honrubia, A first analysis of fast ignition of precompressed ICF fuel by laser-accelerated protons, Nucl. Fus. 42 (2002) L1, http://dx.doi.org/10.1088/0029-5515/42/3/101.

[11] M. Temporal, J.J. Honrubia, S. Atzeni, Numerical study of fast ignition of ablatively imploded deuteriumtritium fusion capsules by ultra-intense proton beams, Phys. Plasmas 9 (2002) 3098, http://dx.doi.org/10.1063/1.1482375.

[12] M. Temporal, Fast ignition of a compressed inertial confinement fusion hemispherical capsule by two proton beams, Phys. Plasmas 13 (2006) 122704, http://dx.doi.org/10.1063/1.2400592.

[13] M. Temporal, J.J. Honrubia, S. Atzeni, Proton-beam driven fast ignition of inertially confined fuels: Reduction of the ignition energy by the use of two proton beams with radially shaped profiles, Phys. Plasmas 15 (2008) 025702, http://dx.doi.org/10.1063/1.2918316.

[14] J.J. Honrubia, J.C. Fernández, B.M. Hegelich, M. Murakami, C.D. Enriquez, Fast ignition driven by quasi-monoenergetic ions: Optimal ion type and reduction of ignition energies with an ion beam array, Laser Part. Beams 32 (2014) 419, http://dx.doi.org/10.1017/S0263034614000305.

[15] J.C. Fernández, J.J. Honrubia, B.J. Albright, K.A. Flippo, D.C. Gautier, et al., Progress and prospects of ion-driven fast ignition, Nucl. Fus. 49 (2009) 065004, http://dx.doi.org/10.1088/0029-5515/49/6/065004.

[16] J.J. Honrubia, J.C. Fernández, M. Temporal, B.M. Hegelich, J. Meyer-ter-Vehn, Fast ignition of inertial fusion targets by laser-driven carbon beams, Phys. Plasmas 16 (2009) 102701, http://dx.doi.org/10.1063/1.3234248.

[17] C.M. Brenner, A.P.L. Robinson, K. Markey, R.H.H. Scott, R.J. Gray, et al., High energy conversion efficiency in laser-proton acceleration by controlling laser-energy deposition onto thin foil targets, App. Phys. Lett. 104 (2014) 081123, http://dx.doi.org/10.1063/1.4865812.

[18] J.C. Fernández, B.J. Albright, F.N. Beg, M.E. Foord, B.M. Hegelich, et al., Fast ignition with laser-driven proton and ion beams, Nucl. Fus. 54 (2014) 054006, http://dx.doi.org/10.1088/0029-5515/54/5/054006.

[19] J.J. Honrubia, M. Murakami, Ion beam requirements for fast ignition of inertial fusion targets, Phys. Plasmas 22 (2015) 012703, http://dx.doi.org/10.1063/1.4905904.

[20] J. Kim, B. Qiao, C. McGuffey, M.S. Wei, P.E. Grabowski, et al., Self-consistent simulation of transport and energy deposition of intense laser-accelerated proton beams in solid-density matter, Phys. Rev. Lett. 115 (2015) 054801, http://dx.doi.org/10.1103/PhysRevLett.115.054801.

[21] P.K. Patel, A.J. Mackinnon, M.H. Key, T.E. Cowan, M.E. Foord, et al., Isochoric heating of solid-density matter with an ultrafast proton beam, Phys. Rev. Lett. 91 (2008) 125004, http://dx.doi.org/10.1103/PhysRevLett.91.125004.

[22] M.H. Key, Status of and prospects for the fast ignition inertial fusion concept, Phys. Plasmas 14 (2007) 055502, http://dx.doi.org/10.1063/1.2719178.

[23] M. Schollmeier, S. Becker, M. Geissel, K.A. Flippo, A. Blazevic, et al., Controlled transport and focusing of laser-accelerated protons with miniature magnetic devices, Phys. Rev. Lett. 101 (2008) 055004, http://dx.doi.org/10.1103/PhysRevLett.101.055004.

[24] K. Harres, I. Alber, A. Tauschwitz, V. Bagnoud, H. Daido, et al., Beam collimation and transport of quasineutral laser-accelerated protons by a solenoid field, Phys. Plasmas 17 (2010) 023107, http://dx.doi.org/10.1063/1.3299391.

[25] I. Hofmann, J. Meyer-ter-Vehn, X. Yan, A. Orzhekhovskaya, S. Yaramyshev, Collection and focusing of laser accelerated ion beams for therapy applications, Phys. Rev. ST Accel. Beams 14 (2011) 031304, http://dx.doi.org/10.1103/PhysRevSTAB.14.031304.

[26] T. Toncian, M. Borghesi, J. Fuchs, E. d'Humières, P. Antici, et al., Ultrafast laser-driven microlens to focus and energy-select mega-electron volt protons, Science 312 (2006) 410, http://dx.doi.org/10.1126/science.1124412.

[27] S. Kar, K. Markey, P.T. Simpson, C. Bellei, J.S. Green, et al., Dynamic control of laser-produced proton beams, Phys. Rev. Lett. 100 (2008) 105004, http://dx.doi.org/10.1103/PhysRevLett.100.105004.

[28] D.T. Offermann, K.A. Flippo, J. Cobble, M.J. Schmitt, S.A. Gaillard, et al., Characterization and focusing of light ion beams generated by ultra-intensely irradiated thin foils at the kilojoule scale, Phys. Plasmas 18 (2011) 056713, http://dx.doi.org/10.1063/1.3589476.

[29] T. Bartal, M.E. Foord, C. Bellei, M.H. Key, K.A. Flippo, et al., Focusing of short-pulse high-intensity laser-accelerated proton beams, Nat. Phys. 8 (2012) 139, http://dx.doi.org/10.1038/nphys2153.

[30] T.D. Arber, K. Bennett, C.S. Brady, A. Lawrence-Douglas, M.G. Ramsay, et al., Contemporary particle-in-cell approach to laser-plasma modelling, Plasma Phys. Control. Fus. 57 (2015) 113001, http://dx.doi.org/10.1088/0741-3335/57/11/113001.

[31] M.H. Key, R.R. Freeman, S.P. Hatchett, A.J. MacKinnon, P.K. Patel, et al., Proton fast ignition, Fus. Sci. Tecnol. 49 (2006) 440.

[32] M.E. Foord, T. Bartal, C. Bellei, M. Key, K. Flippo, et al., Proton trajectories and electric fields in a laser-accelerated focused proton beam, Phys. Plasmas 19 (2012) 056702, http://dx.doi.org/10.1063/1.3700181.

[33] B. Qiao, M.E. Foord, M.S. Wei, R.B. Stephens, M.H. Key, et al., Dynamics of high-energy proton beam acceleration and focusing from hemisphere-cone targets by high-intensity lasers, Phys. Rev. E 87 (2013) 013108, http://dx.doi.org/10.1103/PhysRevE.87.013108.

[34] D.B. Zou, H.B. Zhuo, X.H. Yang, T.P. Yu, F.Q. Shao, et al., Control of target-normal-sheath-accelerated protons from a guiding cone, Phys. Plasmas 22 (2015) 063103, http://dx.doi.org/10.1063/1.4922053.

[35] A. Morace, Fast Ignition: Limits of the Classic Method and Alternative Approaches, Presented at the 14th International Workshop on Fast Ignition and High Field Physics with High Power Lasers, May 17−20, PACIFICO, Yokohama, Japan, 2016.

[36] L. Yin, B.J. Albright, B.M. Hegelich, J.C. Fernández, GeV laser ion acceleration from ultrathin targets: the laser break-out afterburner, Laser Part. Beams 24 (2006) 291, http://dx.doi.org/10.1017/S0263034606060459.

[37] A.P.L. Robinson, M. Zepf, S. Kar, R.G. Evans, C. Bellei, Radiation pressure acceleration of thin foils with circularly polarized laser pulses, New J. Phys. 10 (2008) 013021, http://dx.doi.org/10.1088/1367-2630/10/1/013021.